Computer Methods in Biomechanics and Biomedical Engineering

Publication details, including instructions for authors and subscription information:
http://www.tandfonline.com/loi/gcmb20

Adaptive diffuse domain approach for calculating mechanically induced deformation of trabecular bone

S. Aland [a], C. Landsberg [a], R. Müller [b], F. Stenger [a], M. Bobeth [b], A. C. Langheinrich [c] & A. Voigt [a]

[a] Institut für Wissenschaftliches Rechnen, TU Dresden, 01062, Dresden, Germany

[b] Institut für Werkstoffwissenschaft, TU Dresden, 01062, Dresden, Germany

[c] Diagnostische Radiologie, Universitätsklinikum Giessen/Marburg, 35385, Giessen, Germany

Published online: 15 Mar 2012.

To cite this article: S. Aland, C. Landsberg, R. Müller, F. Stenger, M. Bobeth, A. C. Langheinrich & A. Voigt, Computer Methods in Biomechanics and Biomedical Engineering (2012): Adaptive diffuse domain approach for calculating mechanically induced deformation of trabecular bone, Computer Methods in Biomechanics and Biomedical Engineering, DOI: 10.1080/10255842.2012.654606

To link to this article: http://dx.doi.org/10.1080/10255842.2012.654606

Computer Methods in Biomechanics and Biomedical Engineering
iFirst article, 2012, 1–8

Adaptive diffuse domain approach for calculating mechanically induced deformation of trabecular bone

S. Aland[a], C. Landsberg[a], R. Müller[b], F. Stenger[a], M. Bobeth[b], A.C. Langheinrich[c] and A. Voigt[a]*

[a]*Institut für Wissenschaftliches Rechnen, TU Dresden, 01062 Dresden, Germany;* [b]*Institut für Werkstoffwissenschaft, TU Dresden, 01062 Dresden, Germany;* [c]*Diagnostische Radiologie, Universitätsklinikum Giessen/Marburg, 35385 Giessen, Germany*

(*Received 22 September 2011; final version received 29 December 2011*)

Remodelling of trabecular bone is essentially affected by the mechanical load of the trabeculae. Mathematical modelling and simulation of the remodelling process have to include time-consuming calculations of the displacement field within the complex trabecular structure under loading. We present an adaptive diffuse domain approach for calculating the elastic bone deformation based on micro computer tomogram data of real trabecular bone structures and compared it with a conventional voxel-based finite element method. In addition to allowing for higher computational efficiency, the adaptive approach is characterised by a very smooth representation of the bone surface, which suggests that this approach would be suitable as a basis for future simulations of bone resorption and formation processes within the trabecular structure.

Keywords: adaptive finite elements; diffuse domain approach; trabecular bone; mechanical loading

1. Introduction

The development and therapy of osteoporosis are the subject of continuing intensive investigations. Mathematical modelling and simulation of bone growth can contribute to the understanding of the underlying mechanisms of bone-mass loss and of the characteristic change of the bone mesoscopic architecture. As is well known, bone remodelling is essentially affected by the mechanical loading of the bone. The special pathway of the transduction of mechanical signals to the bone cells is not yet fully understood. Deformation of bone due to external mechanical loading influences the complex interplay between osteocytes, osteoblasts and osteoclasts, where the osteocytes are thought to act as mechanosensors (see e.g. Burger and Klein-Nulend 1999; van der Meulen and Huiskes 2002; Robling et al. 2006; Huang and Ogawa 2010; Jacobs et al. 2010). Numerous studies have been devoted to the modelling of the effect of mechanical loading on bone remodelling, in particular on the evolution of the trabecular bone architecture (e.g. Huiskes et al. 2000; Weinkamer et al. 2004; Ruimerman, Hilbers et al. 2005; Tezuka et al. 2005; Dunlop et al. 2009). Those growth models include bone resorption by osteoclasts and bone formation by osteoblasts, where the bone formation rate depends on the mechanical load in the vicinity of the osteoblasts. In such growth simulations, the calculation of the mechanical load within the trabecular bone structure is rather time consuming. A comparatively fast approximate method ('two-way painting' algorithm) for estimating the mechanical loading within the bone trabeculae has been used in Weinkamer et al. (2004) and Dunlop et al. (2009). For a more accurate calculation of the mechanical bone deformation, the finite element method (FEM) has been applied in Huiskes et al. (2000), Ruimerman, Hilbers et al. (2005) and Tezuka et al. (2005). The base of numerous finite element calculations is the description of the bone morphology by means of a voxel model, which can, for example, easily be derived from a micro computer tomogram (μCT) of the trabecular bone structure. The voxels of the μCT can directly be converted to hexahedral finite elements. This leads to an artificial voxel-roughness of the bone surface. To achieve high resolution of the bone surface, a large number of sufficiently small voxels are necessary. Finite element calculations of the bone deformation on the base of such a hexahedral mesh, naturally given from the μCT, are rather time consuming because of the large number of degrees of freedom. In particular, this slows down simulations of bone growth where the mechanical bone deformation has to be newly calculated all the time due to the permanently changing bone structure. In addition to the computational demand, the approach leads to non-smooth surfaces. Subsequent smoothing might lead to distorted elements and thus possibly to a corruption of the results. As an alternative, unstructured tetrahedral meshes can be used to resolve the trabecular bone structure. This, however, remains a non-trivial task for complicated domains.

In this paper, we will present an alternative method for calculating the mechanical loading of trabecular bone structures by constructing an appropriate adaptive finite element mesh of a domain in which the bone is embedded.

*Corresponding author. Email: axel.voigt@uni-dresden.de

ISSN 1025-5842 print/ISSN 1476-8259 online

http://dx.doi.org/10.1080/10255842.2012.654606
http://www.tandfonline.com

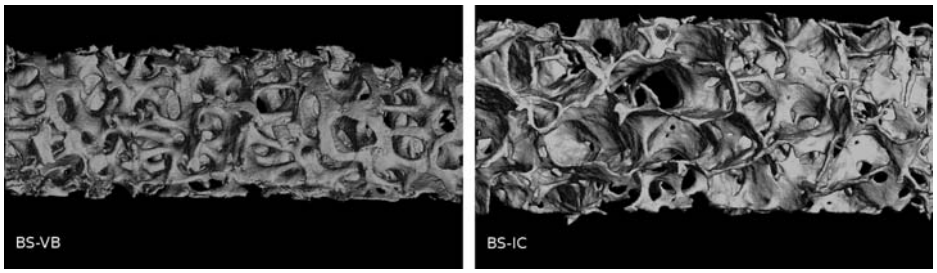

Figure 1. Bone specimen (BS-VB) from a vertebral body demonstrates regular bone architecture (left), whereas bone specimen (BS-IC) from iliac crest shows severe osteoporosis (right). Both are confirmed by histopathology.

A resolution on a voxel scale is no longer needed over the whole sample. Instead the geometry is described implicitly using a phase-field function, which allows an efficient meshing of the trabecular bone structure. Such a diffuse domain approach has been introduced in Li et al. (2009) and applied to various fields, as, for example, chemotaxis in scaffolds (Landsberg et al. 2011), heat transfer in foams and fluid flow in microfluidic applications (Aland et al. 2010).

The aim of the present investigation is to demonstrate the feasibility of the adaptive diffuse domain method for calculating the mechanical loading of trabecular bone structures. This will be done for specimens obtained as sections of real trabecular bone. Representative parts of these specimens will be subjected to artificial overall deformations, which are thought to roughly resemble typical loading situations of the trabecular bone.

This paper is outlined as follows. First, the origin and imaging of the special bone specimens considered here are briefly described. For completeness, we present then the basic equations of elastostatics for isotropic material properties together with the special boundary conditions posed on the bone specimens. After describing the adaptive diffuse domain finite element approach, the results and the computational efficiency of the method are analysed.

2. Pre-processing

2.1. Micro-computed tomography

Two human bone specimens obtained for diagnostic purposes from two different patients were obtained from the Giessen Institute of Pathology, see Figure 1. Samples were scanned en bloc by a μCT system (SkyScan1072 80 kV, Belgium) described recently (Langheinrich et al. 2004). The specimens were rotated at angular increments of 0.45° and scanned 180° around the vertical axis at 60 kVp. Acquisition time for each view was 2.4 s. The relative position of the object to the source determines geometric magnification and thus the pixel size explained by the cone-beam geometry of the system. Maximum possible magnification is limited by the specimen size, which has to be within the cone-beam in its horizontal diameter. We used high geometric magnification up to 80×. The volume images were reconstructed from the angular views using a modified Feldkamps filtered back projection (Feldkamp et al. 1989). The radiopacity of each voxel used for image analysis and display was represented by an 8-bit greyscale value. For this study, the μCT scanner was configured so that the side dimension of the cubic voxels was 8.0 μm for specimen BS-IC and 9.8 μm for BS-VB (8-bit greyscale, see Figure 1). Next, the resulting volume data-sets were binarised as reported previously (Litzlbauer et al. 2010).

2.2. Implicit representation of volume data

Starting from the tomographic image of the bone structure, we cut out a cuboid $\Omega = [0, a] \times [0, a] \times [0, c]$ where the integers a and c define the size of the 3D image in voxels. The region containing the solid bone Ω_1 within the cuboid Ω is then defined by white voxels in the binarised data-set.

Instead of explicitly defining the complicated domain prescribing the bone material Ω_1, we follow the ideas of Li et al. (2009) using the so-called diffuse domain approach. This allows to solve the governing equations in the regular cuboidal domain Ω by using a phase-field describing the interior domain Ω_1 implicitly. We introduce the phase-field function ϕ to smoothly approximate the geometry of Ω_1: $\phi \approx 1$ in Ω_1 and $\phi \approx 0$ in $\Omega \backslash \Omega_1$. Here, we use

$$\phi(\mathbf{x}) = 0.5(1 - \tanh(3r(\mathbf{x})/\varepsilon)), \tag{1}$$

where $r(\mathbf{x})$ is the signed distance from a point $\mathbf{x} \in \Omega$ to the interior boundary $\Gamma_1 := \partial\Omega_1 \backslash \partial\Omega$, see Figure 2 (left) for an illustration. The thickness of the boundary transition layer is given by ε. Accordingly, the sharp boundary of the original domain is replaced by a narrow diffuse interface layer.

We generate the signed distance function from the given voxel data. For details see Landsberg et al. (2011). The regular cuboidal domain Ω is triangulated using tetrahedral elements which are locally refined according to the phase-field function ϕ. Figure 2 (right) shows an example of the adaptively refined mesh.

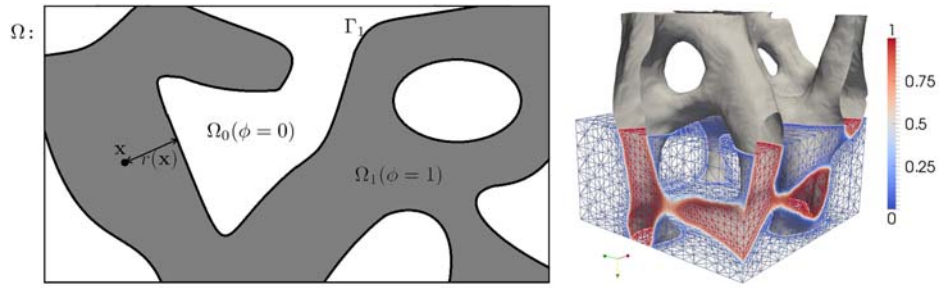

Figure 2. (Left) Schematic representation of the domains. The cuboid Ω is divided into the two regions Ω_0 and Ω_1 and the interior boundary Γ_1. (Right) The 0.5-level set contour of the phase-field ϕ (upper region) and finite element mesh coloured by the value of ϕ (lower region) of the phase-field ϕ. Colour online.

3. Mathematical model

In this work, we assume that the mechanical stimulation of trabecular bone growth occurs via the elastic deformation of the trabeculae. The effect of the bone marrow between the trabeculae on the bone deformation is completely neglected. For the following calculations, the mechanical material properties of the trabeculae are supposed to be isotropic with Young's modulus $E = 10\,\text{GPa}$ and Poisson's ratio $\nu = 0.17$, see Heinemann (2010). The bone deformation is described by the displacement vector $\mathbf{u}$ obeying the partial differential equation

$$\nabla \cdot \sigma = 0 \quad \text{in } \Omega_1, \tag{2}$$

with the stress tensor

$$\sigma = \mu(\nabla \mathbf{u} + \nabla \mathbf{u}^T) + \lambda I \nabla \cdot \mathbf{u}, \tag{3}$$

where I is the identity matrix, and μ and λ are the Lamé coefficients

$$\mu = \frac{E}{2(1+\nu)}, \quad \lambda = \frac{E\nu}{(1+\nu)(1-2\nu)}.$$

The overall mechanical loading of a trabecular bone structure depends on its special location within the whole bone and on the external loading of the bone under consideration. The trabecular architecture naturally adapts to the typical loading situation. For demonstrating our numerical method, we disregard here the actual loading of the bone specimen and consider a simple artificial loading, corresponding to a compression of the trabecular bone. From the cylindrical bone specimens shown in Figure 1, we had cut prismatic sections. The coordinate system is chosen parallel to the edges of the quadratic prism with side lengths $a \times a \times c$. The trabeculae are cut along the prism faces. On all surfaces of the cut trabeculae within the six faces of the quadratic prism, we set all components of the displacement vector as if it was a homogenous block of material. Introducing the components u, v, w of the displacement vector $\mathbf{u}^T = (u, v, w)$, this means

$$u|_{\partial\Omega} = \bar{\varepsilon}_x x, \quad v|_{\partial\Omega} = \bar{\varepsilon}_y y, \quad w|_{\partial\Omega} = \bar{\varepsilon}_z z,$$

where $\bar{\varepsilon}_x$, $\bar{\varepsilon}_y$ and $\bar{\varepsilon}_z$ are the mean strains in the corresponding directions. These mean strains are differently chosen for the two specimens under consideration. In the case of the specimen from a vertebral body (BS-VB), the values $\bar{\varepsilon}_x = \bar{\varepsilon}_z = -1800$ μstrain and $\bar{\varepsilon}_y = -2000$ μstrain are adopted. Such a compressive deformation in all directions is thought to be caused by the special form of vertebral bodies (cf. Weinkamer et al. 2004). For the specimen from iliac crest (BS-IC), a mean deformation with $\bar{\varepsilon}_z = -2000$ μstrain and $\bar{\varepsilon}_x = \bar{\varepsilon}_y = 340$ μstrain is considered, which resembles a uniaxial compression with an effective Poisson's ratio of trabecular bone of $\nu = 0.17$ (van Rietbergen et al. 1998; Park et al. 2007). A similar specimen deformation (compressive in vertical and tensile in horizontal directions) has been considered, for example, in Ruimerman, Hilbers et al. (2005), in which, however, the loads instead of displacements were imposed. As further boundary condition we require vanishing traction forces on the bone surfaces within the prism.

Using the diffuse domain approach, the governing equations can be rewritten as

$$\nabla \cdot (\phi\sigma) = 0. \tag{4}$$

This equation is now valid in the domain Ω. Using finite elements, we end up with the discrete weak formulation

$$\int_\Omega \phi\mu(\nabla \mathbf{u}_h + \nabla \mathbf{u}_h^T) \cdot \nabla \eta \, \mathrm{d}x + \int_\Omega \phi\lambda \nabla \cdot \mathbf{u}_h \nabla \eta \, \mathrm{d}x = 0, \tag{5}$$

where the Dirichlet boundary conditions have to be incorporated into the discrete solution $\mathbf{u}_h$ and the test functions η. Using matched asymptotic expansion, the reformulated equation can be shown to converge to the original model and boundary conditions as the width of the diffuse interface layer tends to zero (see Li et al. 2009).

To discretise the system, we use piecewise linear finite elements within the adaptive finite element toolbox *AMDiS*

(Vey and Voigt 2007). As numerical value for the interface width we use $\varepsilon = 85\,\mu m$ for specimen BS-VB and $\varepsilon = 32\,\mu m$ for BS-IC. The different values result from different geometric structures and are chosen such that the smallest features can be resolved. Numerical tests on benchmark problems show the independency of the solution on ε, see Li et al. (2009). The mesh is refined along the boundary Γ such that approximately five grid points are across the diffuse interface. In the case of the voxel-based calculations, piecewise linear hexahedral elements are used which correspond to the voxels of the μCT.

4. Calculated bone deformation

As already mentioned in the introduction, the mechanisms of mechanosensing and signal transduction to bone cells are not precisely known. In particular, it is not clear which mechanical quantity is sensed by the cells, especially by the osteocytes. In previous studies the strain energy density (Ruimerman, Hilbers et al. 2005; van Rietbergen, Weinans et al. 1995) and the relative volume change (trace of the strain tensor or volumetric strain; van Rietbergen, Weinans et al. 1995; Dunlop et al. 2009) have been considered as relevant mechanical quantities. For brevity, we use in the following term volumetric strain (Ruimerman, van Rietbergen et al. 2005) for the trace of the strain tensor. A comprehensive comparative analysis of different mechanical quantities has been carried out in van Rietbergen, Weinans et al. (1995) in which the strain energy density, maximal principle strain and the volumetric strain were used in simulations of bone modelling and remodelling. In addition, also the spatial gradients of these quantities were considered as relevant mechanical variables. One of the unclear points of the mechanosensory transduction in bone is to what extent the osteocytes respond directly to bone deformation in their immediate vicinity or whether they respond also to fluid flow within the canalicular network connecting theosteocytes in the bone (Burger and Klein-Nulend 1999; van der Meulen and Huiskes 2002; Robling et al. 2006; Huang and Ogawa 2010; Jacobs et al. 2010). In the latter case, the spatial gradient of the volumetric strain would be more relevant for driving fluid flow to trigger bone growth. Near the bone surface, the flow from canaliculi to the bone marrow (or vice versa) is also directly driven by the volumetric strain within the trabeculae. For demonstration purposes, we consider here the volumetric strain as a relevant quantity for mechanosensing. All other mechanical quantities mentioned above can easily be derived from the calculated displacement field.

Figures 3 and 4 show comparisons of the displacement fields for the two examples of human bone specimens, calculated by the two numerical approaches. Figure 3 displays all three displacement components for the case of the regular bone structure (BS-VB). For the osteoporotic specimen (BS-IC), only the z-component of the displacement is shown (Figure 4). The coloured images are in good agreement. Note that the representation of the bone morphology within the diffuse domain approach exhibits very smooth surfaces, whereas for the other approach a certain voxel-roughness is visible. All images are generated by means of the software Paraview (www.paraview.org). Figure 5 shows line plots of the z-component of the displacement fields along the body diagonal of the specimen for the more complex structure BS-IC. The diagram generally reveals differences of less than 1% between the two methods. The single spot with larger differences corresponds to a very small piece of bone, which is not sufficiently resolved by the used meshes.

To summarise, the adaptive diffuse domain approach and the voxel-based FEM show good agreement. The geometries of the considered domains in the two approaches differ only within the scale of one voxel and differences in the displacements are mostly less than 1%, at isolated spots less than 5%. However, the computational effort for calculating the displacement field is reduced within the diffuse domain approach compared to the voxel-based FEM (see Table 1). In case of the bone specimen BS-IC, the use of an adaptive mesh leads to the reduction in the number of degrees of freedom by a factor of 2. For specimen BS-VB, by using a coarser mesh, the number of degrees of freedom decreases by a factor of 18, while still yielding reasonable results.

As an example for a derived mechanical quantity, which is thought to be related to the sensing of the mechanical load by the osteocytes, the volumetric strain, computed with both methods, is shown in Figure 6 for the case of the osteoporotic bone specimen (BS-IC) with very thin trabeculae. The coloured images are again in good agreement. The image reveals localised regions of highly strained trabeculae where a comparatively large mechanical signal should trigger enhanced bone growth. Also a line plot of the volumetric strain along a body diagonal of the specimens generally shows good quantitative agreement of the methods within few percents, except for very thin trabeculae (Figure 7).

5. Conclusions

The described diffuse domain approach provides an efficient alternative to voxel-based finite element calculations with the advantage to deal with smooth surfaces. Furthermore, the approach only requires standard numerical techniques. Starting from volume data-sets of a μCT scanner, an implicit representation of the geometry can be computed and used to represent the domain of interest within the computational model. Combined with

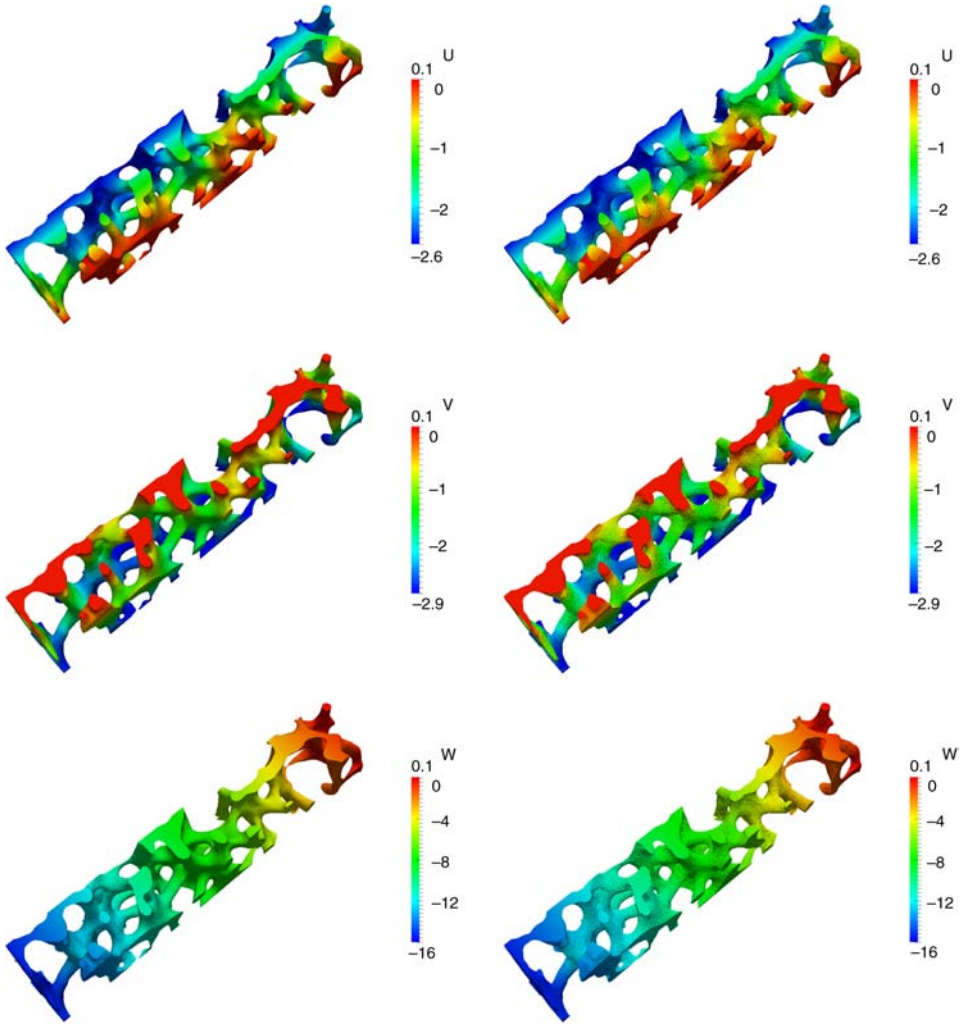

Figure 3. Bone specimen BS-VB: the three components of the displacement field **u** from top to bottom. (Left) Results obtained with adaptive diffuse domain approach; (right) results obtained using voxel FEM. Colour online.

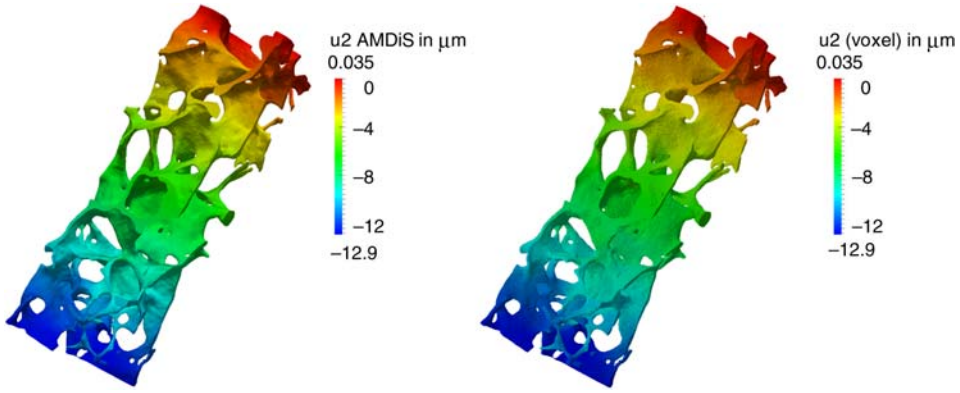

Figure 4. Bone specimen BS-IC: comparison of the z-component of the displacement fields **u**, calculated with the adaptive diffuse domain approach (left) and the voxel-based FEM (right). Colour online.

Table 1. Comparison of the number of degrees of freedom between the adaptive diffuse domain approach and the voxel-based FEM (MDOFs – million degrees of freedom).

Specimen	Method	MDOFs
BS-VB	Diffuse domain	0.9
	voxel-based FEM	16.7
BS-IC	Diffuse domain	6.4
	voxel-based FEM	14.3

Note: For the calculation on specimen BS-VB a coarse mesh was used, demonstrating the capability of the phase-field method to adapt computational effort to desired accuracy.

an adaptive mesh refinement algorithm, the method also allows for fast multilevel solvers and thus scales on parallel systems. With the available computing power of high performance computers, this will allow to resolve large bone specimens. The accuracy and efficiency of the approach which is demonstrated here only for a linear elasticity problem with isotropic material are expected to remain for non-isotropic and nonlinear behaviour.

Due to the potential computational efficiency and the smooth representation of the trabecular bone surface, the presented phase-field approach seems to be suited as base

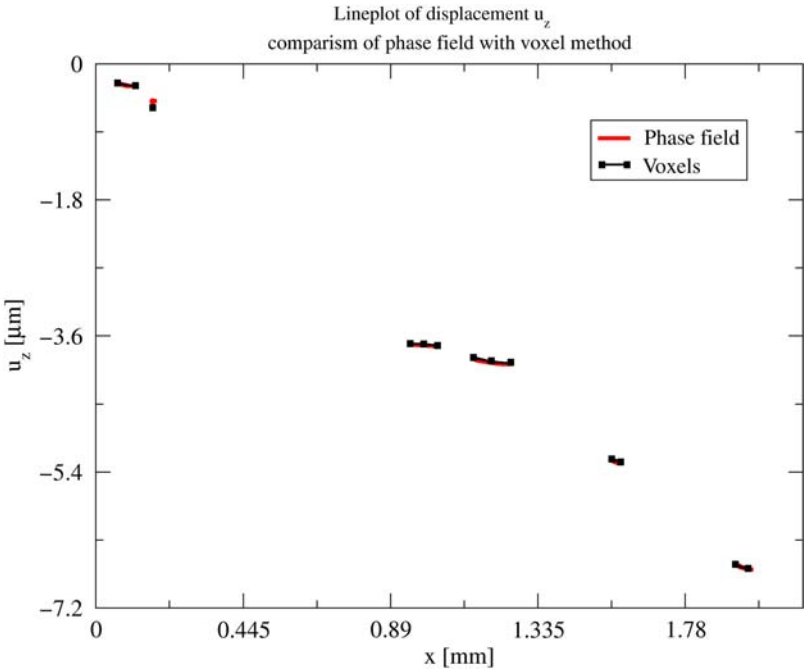

Figure 5. Bone specimen BS-IC: comparison of line plots of the z-component of the displacement fields $\mathbf{u}$, calculated with the adaptive diffuse domain approach and the voxel-based FEM. The diagram reveals good quantitative agreement.

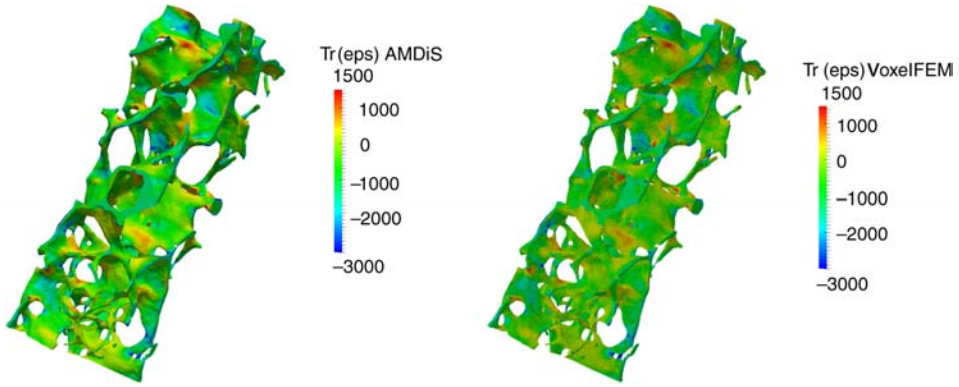

Figure 6. Comparison of the volumetric strain for the deformation of the osteoporotic bone specimen BS-IC calculated with the adaptive diffuse domain approach (left) and the voxel-based FEM (right). The picture reveals localised regions of highly strained trabeculae. The colour bar is cut to the shown range. Colour online.

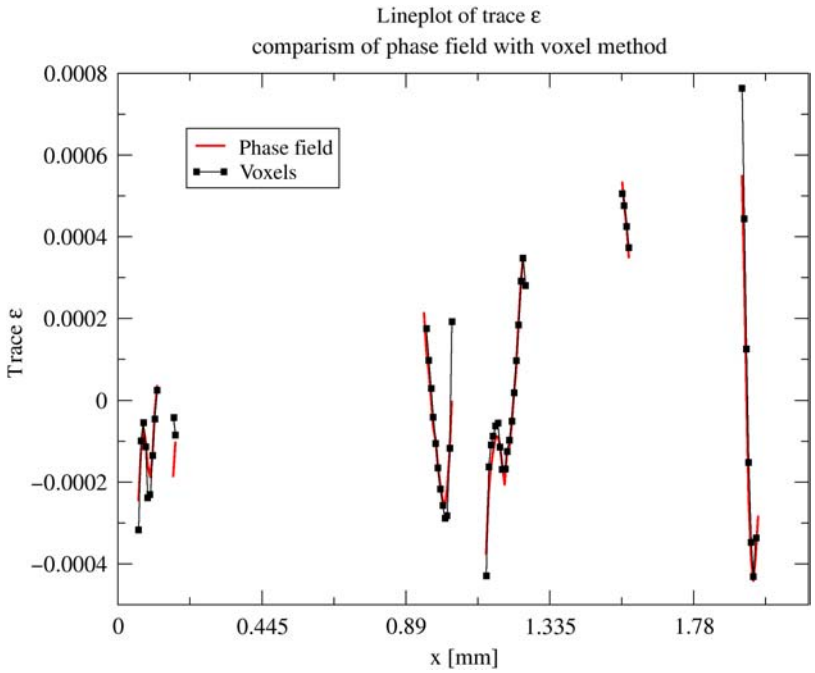

Figure 7. Bone specimen BS-IC: comparison of line plots of the volumetric strain for the deformation of the osteoporotic bone specimen BS-IC calculated with the adaptive diffuse domain approach and the voxel-based FEM. The diagram shows good quantitative agreement of the strains.

for future simulations of the remodelling of trabecular bone. The evolution of the bone surface of the trabeculae due to bone resorption and formation processes could favourably be described within a phase-field theory.

Acknowledgements

We thank the Center for Information Services and High Performance Computing (ZIH) at the Dresden University of Technology for computational resources. The study has been supported by the Deutsche Forschungsgemeinschaft (DFG) through SFB/TR 79 sub-project M8.

References

Aland S, Lowengrub J, Voigt A. 2010. Two-phase flow in complex geometries: a diffuse domain approach. CMES. 57: 77–108.

Burger EH, Klein-Nulend J. 1999. Mechanotransduction in bone – role of the lacuno-canalicular network. FASEB J. 13(Suppl.):S101–S112.

Dunlop JWC, Hartmann MA, Brechet YJ, Fratzl P, Weinkamer R. 2009. New suggestions for the mechanical control of bone remodeling. Calcif Tissue Int. 85(1):45–54.

Feldkamp L, Goldstein SA, Parfitt AM, Jension G, Kleerekoper M. 1989. The direct examination of three-dimensional bone architecture *in vitro* by computed tomography. J Bone Miner Res. 4(1):3–11.

Heinemann S. 2010. Entwicklung und Charakterisierung biokompatibler Kompositxerogele im System Silikat-Kollagen-Calciumphosphat für den Knochenersatz. Dissertation. TU Dresden.

Huang C, Ogawa R. 2010. Mechanotransduction in bone repair and regeneration. FASEB J. 24(10):3625–3632.

Huiskes R, Ruimerman R, van Lenthe G, Janssen JD. 2000. Effects of mechanical forces on maintenance and adaptation of form in trabecular bone. Nature. 405(8):704–706.

Jacobs CR, Temiyasathit S, Castillo AB. 2010. Osteocyte mechanobiology and pericellular mechanics. Annu Rev Biomed Eng. 12:369–400.

Landsberg C, Stenger F, Deutsch A, Gelinsky M, Rösen-Wolff A, Voigt A. 2011. Chemotaxis of mesenchymal stem cells within 3D biomimetic scaffolds – a modeling approach. J Biomech. 44(2):359–364.

Langheinrich AC, Bohle RM, Greschus S, Hackstein N, Walker G, von Gerlach S, Rau WS, Holschermann H. 2004. Atherosclerotic lesions at micro CT: feasibility for analysis of coronary artery wall in autopsy specimens. Radiology. 231(3):675–681.

Li X, Lowengrub J, Rätz A, Voigt A. 2009. Solving PDE's in complex geometries. Comm Math Sci. 7(1):81–107.

Litzlbauer HD, Korbel K, Kline TL, Jorgensen SM, Eaker DR, Bohle RM, Ritman EL, Langheinrich AC. 2010. Synchrotron-based micro-CT imaging of the human lung acinus. Anat Rec (Hoboken). 293:1607–1614.

Park YH, Cha HS, Hong J. 2007. Microscopic multi-directional mechanical properties of human femoral cancellous bone tissue. Key Eng Mater. 342–343:13–16.

Robling AG, Castillo AB, Turner CH. 2006. Biomechanical and biomolecular regulation of bone remodelling. Annu Rev Biomed Eng. 8:455–498.

Ruimerman R, Hilbers P, van Rietbergen B, Huiskes R. 2005. A theoretical framework for strain-related trabecular bone maintenance and adaptation. J Biomech. 38(4):931–941.

Ruimerman R, van Rietbergen B, Hilbers P, Huiskes R. 2005. The effects of trabecular-bone loading variables on the surface signaling potential for bone remodeling and adaptation. Ann Biomed Eng. 33(1):71–78.

Tezuka K, Wada Y, Takahashi A, Kikuchi M. 2005. Computer-simulated bone architecture in a simple bone-remodeling model based on a reaction-diffusion system. J Bone Miner Metab. 23(1):1–7.

Van der Meulen MCH, Huiskes R. 2002. Why mechanobiology? A survey article. J Biomech. 35(4):401–414.

Van Rietbergen B, Majumdar S, Pistoia W, Newitt DC, Kothari M, Laib A, Rüegsegger P. 1998. Assessment of cancellous bone mechanical properties from micro-FE models based on micro-CT, pQCT and MR images. Technol Health Care. 6(5–6):413–420.

Vey S, Voigt A. 2007. AMDiS – adaptive multidimensional simulations. Comput Vis Sci. 10(1):57–67.

Weinkamer R, Hartmann MA, Brechet Y, Fratzl P. 2004. Stochastic lattice model for bone remodeling and aging. Phys Rev Lett. 93(22):228102-1–228102-4.